frontiers in Marine Science

ORIGINAL RESEARCH
published: 02 November 2021
doi: 10.3389/fmars.2021.746773

Paleo-Typhoon Events as Indicated by Coral Reef Boulder Deposits on the Southern Coast of Hainan Island, China

Liang Zhou[1], *Shu Gao*[2]*, *Jianjun Jia*[3], *Yang Yang*[4], *Changliang Tong*[5] *and Aijun Wang*[6]

[1] School of Geography, Geomatics, and Planning, Jiangsu Normal University, Xuzhou, China, [2] Ministry of Education Key Laboratory for Coast and Island Development, Nanjing University, Nanjing, China, [3] State Key Laboratory of Estuarine and Coastal Research, East China Normal University, Shanghai, China, [4] School of Marine Science and Engineering, Nanjing Normal University, Nanjing, China, [5] Marine Geological Institute of Hainan Province, Haikou, China, [6] Open Laboratory for Coast and Ocean Environmental Geology, Third Institute of Oceanography of Ministry of Natural Resources (MNR), Xiamen, China

The southern coast of Hainan Island, China, is one of the most frequently hit areas of tropical cyclones in the Northwest Pacific regions. Although some of the extreme typhoon events were known in historical times, quantitative information on the timing and magnitude of paleo-typhoon events in this coastal area remains rare. In the present study, a large number of coral reef boulders were found on the Xiaodonghai reef platform, on the south coast of Hainan Island. Morphometric analysis of the boulders shows an exponentially fining landward trend, indicating a storm origin; a wave-induced current velocity of 2.41–5.71 m/s during the storm events is required to transport the boulders that were originally situated outside the reef edge. Based on the U/Th and ^{14}C dating for the age-indicating samples taken from the boulders, seven major periods with intense typhoon activities were identified for the last 4,000 years, i.e., 1800–1500 BCE, 1200–900 BCE, 50–120 CE, 550–800 CE, 900–1000 CE, 1350–1900 CE, and 1910–2000 CE. A comparison with the regional typhoon records in terms of climatic parameters in the northwestern Pacific and the South China Sea regions indicates that the longitudinal variations of intense typhoon frequency were mainly controlled by El Niño-Southern Oscillation (ENSO), dominantly modulated by the Intertropical Convergence Zone. Because of the future warming climate, there will be a trend of enhanced typhoon risk for the southern Hainan Island coasts.

Keywords: coral reef boulders, typhoon events, spatial variations, climatic factors, Hainan Island coasts

OPEN ACCESS

Edited by:
Juan Jose Munoz-Perez, University of Cádiz, Spain

Reviewed by:
Helena Granja, University of Minho, Portugal
Liqin Zuo, Nanjing Hydraulic Research Institute, China

***Correspondence:**
Shu Gao
shugao@nju.edu.cn

Specialty section:
This article was submitted to Coastal Ocean Processes, a section of the journal Frontiers in Marine Science

Received: *24 July 2021*
Accepted: *01 October 2021*
Published: *02 November 2021*

Citation:
Zhou L, Gao S, Jia J, Yang Y, Tong C and Wang A (2021) Paleo-Typhoon Events as Indicated by Coral Reef Boulder Deposits on the Southern Coast of Hainan Island, China. Front. Mar. Sci. 8:746773. doi: 10.3389/fmars.2021.746773

INTRODUCTION

Intense tropical cyclones (TCs) are among the deadliest natural disasters for the populations inhabiting coastal areas. Because of rapid infrastructure expansion and urban growth in coastal areas, more people and their assets are being exposed to extreme wave events, which enhances the societal vulnerability and risk, as indicated by recent life and economic losses (Von Storch and Reichardt, 1997; Gönnert and Birgit, 2015; Vousdoukas et al., 2016). Any significant change in the frequency and/or intensity of coastal TCs due to climate change is likely to have a notable impact on the economic prosperity of coastal areas. For East Asian coastal "megacities" and tourist

hotspots in particular, such as Guangzhou, Macau, Hong Kong, Sanya, Tokyo, and Seoul, the potential exposure is a legitimate concern (Nadin et al., 2016). On the other hand, predicting the frequency and magnitude of large typhoons in the region in the background of global warming are relatively rare, especially for the northern coastlines of the South China Sea. The need for coastal risk assessment, raising societal awareness, and preparation to prevent the possible adverse impacts of large storm events are therefore critical for East Asian coastal populations. However, short meteorological records and incomplete historical documentation may lead to imprecision in the estimation of typhoon disaster risk (Suursaar et al., 2015).

As such, geological records offer a great potential to predict the future trend of coastal typhoon activity. Emerged coastal boulder deposits are widely recognized as an effective indicator of large storm events (Nott, 1997, 2000, 2003; Goff et al., 2006; Imamura et al., 2008; Barbano et al., 2010; Nandasena et al., 2011, 2013). The study of coastal boulder deposits has become a new research hotspot at the intersection of coastal geomorphology and marine hazards (e.g., Paris et al., 2011; Etienne, 2012; Naylor et al., 2016). Their application can be summarized as follows: (a) A detailed study of the features of coastal boulder deposits (e.g., size, shape, position, and rock density) may be able to distinguish different types of high-energy hydrological events (e.g., storms and tsunamis; Nott, 1997, 2003; Goto et al., 2010; Lorang, 2011; Cox et al., 2012; Nakamura et al., 2014); (b) Investigating sedimentological properties and spatial variations of coastal boulders may provide a way of interpreting morphodynamic behavior over longer timeframes (Chen et al., 2011; Paris et al., 2011; Naylor et al., 2016); (c) Carbon boulder deposits (CBDs) have been successfully used to determine the frequency of large TCs (Banerjee et al., 2001; Lau et al., 2016; Kitamura et al., 2017); and (d) Climatic variability may imply hydrological changes with more frequent large storm events, and thus investigations of large storm events in coastal zones may allow linkages with climate change over the long term time-scales (Yu et al., 2009, 2012; Lau et al., 2016; Zhou et al., 2019a,b; Zhou X. et al., 2019).

Hainan Island is located in the northern part of the South China Sea (SCS). It has experienced dramatic growth in tourism since the post-1979 reforms in China. In popular tourist destinations such as Sanya, densely populated urban constructions are widely distributed in the coastal lowland. At the same time, Hainan Island is susceptible to TCs with an average of 5–7 TCs per year according to observations (Wu et al., 2007; Wang et al., 2012). Zhou and Adams (1988) claimed that the South China Sea has the highest tsunami risk in China, however, Mak and Chan (2007) noted that Hainan Island has experienced very few historical tsunamis. At Sanya in southern Hainan Island, numerous CBDs are distributed on the reef flat and on land (**Figure 1**). These boulder fields are ideal sites for research into coastal large typhoon events.

This study aimed to map and characterize coastal CBDs on the Sanya coast to address the following key questions: (1) the magnitude of the typhoon events required to transport them to their present positions, and (2) the effects of different climatic regimes on SCS large typhoon in temporal and spatial variations.

Study Area

The Xiadonghai embayment, the area for the present study, is near Luhuitou on the south coast of Hainan Island (**Figure 1**). Tides here are irregularly diurnal, with a mean tidal range of 0.85 m (State Oceanic Administration, 1999) and a weak tidal current, i.e., generally 0.1–0.2 m/s. The local wave climate is seasonal and highly influenced by typhoon activity with around 80% of waves approaching the coast from East South East (ESE) to West South West (WSW) directions. The average wave height range is 0.6-0.8 m, and the wave period range is 2.5–3.5 s (State Oceanic Administration, 1999). Storminess is a feature of the wet season from March to November. In general, ∼five typhoons (at least three being very strong) hit this coast per year. A maximum summer wind velocity of 45 m/s was recorded during Typhoon Kelly (Wang et al., 1998). Typhoon Elaine on October 9, 1971, produced a maximum storm surge, reaching 3.92 m above chart datum (Wang et al., 1998). Reliable measurements and documentation for typhoon wave data are only back to the 1980s in the study area. By extrapolating the typhoon wave data for Hainan Island (22 years of observations), maximum significant typhoon wave heights are calculated as ∼4.84 m every 2 years, 9.51 m every 50 years, 10.80 m every 100 years (Yao et al., 1991), and 18.7 m every 200 years (Yin, 2014).

Xiaodonghai (XDH) belongs to the Sanya national coral reef reserve. The reef flat is ∼300 m wide and >1,800 m long. A back-reef moat of 1 m average depth lies between the reef crest and beach. The deepest parts of the moat reach 1–2 m but become shallow (70 cm) during low tide when the reef crest and much of the moat (trough) dry up (Zhang, 2001).

METHODS

Field Survey and Measurements

In situ investigations at the XDH study site were carried out in December 2016 during low spring tides. Most of the boulders are apparently derived from the reef front, as generally shown by their overlapping erosional marine features, barnacles on their upper surface, and other faces with a freshly cut appearance. For the boulders on the reef flat with a long axis length of >0.5 m, we measured the dimensions of long (a), intermediate (b), and short (c) axes, and the long axis directions. The positions and elevations of CCBs were measured using an RTK–GPS survey System, at a vertical and horizontal accuracy of ±1.5 and ±1 cm, respectively. In total, 1247 CBDs were measured in the field.

Small pieces were collected from 42 typical boulders for the estimation of bulk density, carried out at the laboratory using the following equation:

$$\rho_b = \rho_w\left(\frac{W_a}{W_a - W_f}\right) \quad (1)$$

where ρ_b is the boulder bulk density, ρ_w is the seawater density (1.02 g/cm^3), W_a is the boulder weight in the air, and W_f is the boulder submerged weight in seawater.

As CBDs are often irregular and non-rectangular in shape, their volumes (V) were estimated using the following equations

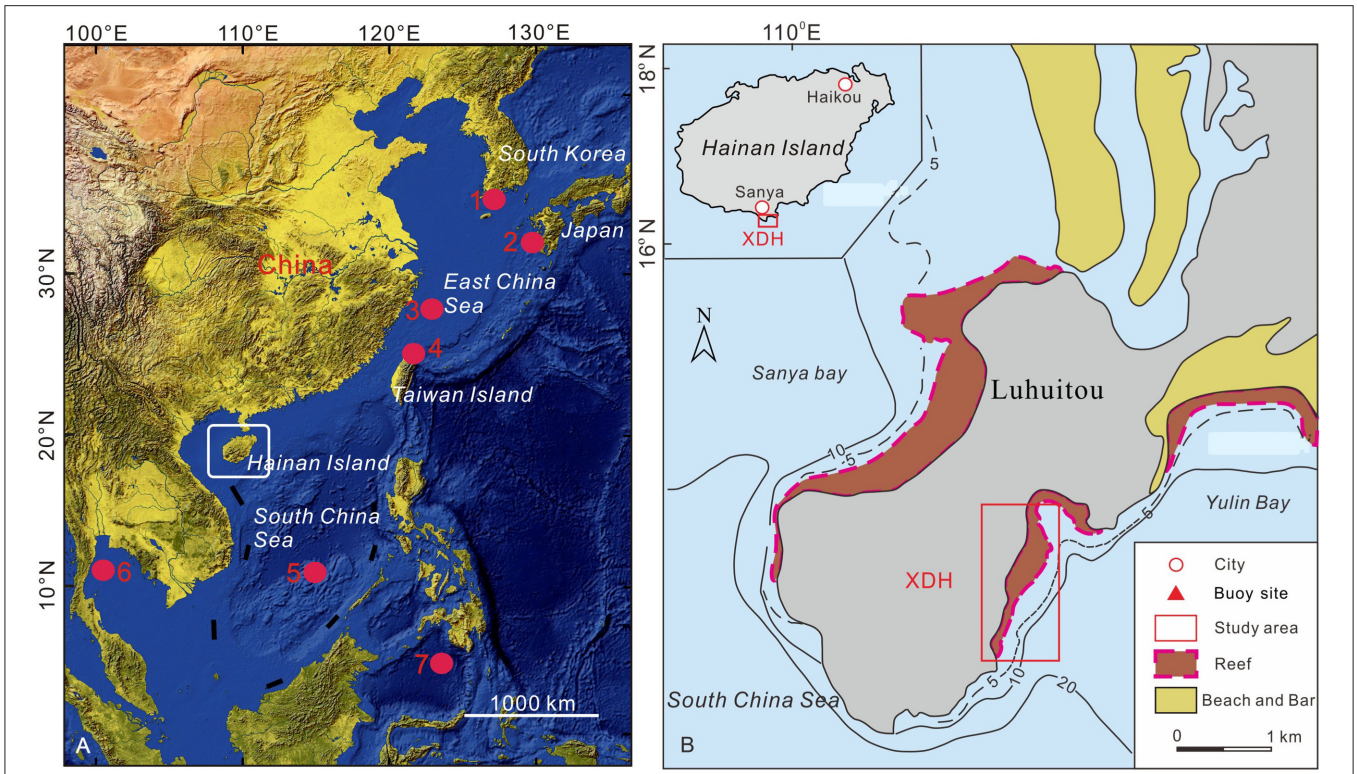

FIGURE 1 | (A) Location of Hainan Island in the northern South China Sea. Shown also here are the sites of (1) South Korea (Yang et al., 2017), (2) Kamikoshiki Island in Japan (Woodruff et al., 2009), (3) East China Sea (Zhou X. et al., 2019), (4) Taiwan (Chen et al., 2012), (5) the Yongshu Reef of southern SCS (Yu et al., 2004), (6) Gulf of Tailand (Terry et al., 2018), and (7) core MD98-2181 (Stott et al., 2004), where additional information was used in this study. **(B)** The coastline of Luhuitou showing the maximum extent of reefs and the study site at Xiaodonghai [modified from Zhao et al. (1983), Zhang (2001)].

to avoid over-estimation (Lau et al., 2016):

$$Triangular boulders: V = 0.5(a \times b \times c) \quad (2)$$

$$Ellipsoidal boulders: V = \frac{4}{3}\pi\left(\frac{a \times b \times c}{8}\right) \quad (3)$$

$$Rectangular boulders: V = 0.7(a \times b \times c) \quad (4)$$

For the larger boulders (a>2 m), we also use a Riegl VZ-4000 terrestrial laser scanner to measure the boulder volume which was calculated by a direct point-to-point cloud comparison method (Xie et al., 2017).

Boulder mass was estimated as the product of volume and bulk density. The bulk density was carried out on 10 selected coral samples and calculated as 1.82 t m^{-3} based on Equation (1).

Boulder Morphology Statistics

The morphology of sedimentary particles [e.g., maximum projection sphericity (MPS), oblate prolate index (OPI), disc–rod index (DRI), and roundness] is widely recognized as an important source of information on sediment provenance, transport, and dynamic environment (**Table 1**; Dobkins and Folk, 1970; Pettijohn et al., 1987; Illenberger, 1991; Wang et al., 2004; Chen et al., 2011). OPI is a useful index for differentiating oblate from prolate boulder shapes. MPS reflects the balance of drag and gravitational forces acting on a particle immersed in a fluid and, as such, is an important index of the behavior of particles transported by or settling in the water. DRI is effective in distinguishing rod-shaped from disc-shaped boulders.

TABLE 1 | Calculation methods of boulder shape parameters.

Index	Formula	References
MPS	$[c^2/(a \times b)]^{1/3}$	Sneed and Folk, 1958
OPI	$10 \times [(a-b)/(a-c) - 0.5]/(c/a)$	Dobkins and Folk, 1970
DRI	$(a-b)/(a-c)$	Illenberger, 1991

The Critical Current Velocity for Boulder Movement

Coral boulders on the Yulin Bay reef flat originated from two possible sources (**Figures 2**, **3**, **5**): (1) the active reef edge or reef slope (collectively called "reef-edge boulders") and (2) from mid-Holocene emerged reef remnants or other emerged features (collectively called "emerged reef boulders"). When a boulder exhibited a surface appearance resembling that of the remnant reef at the locality and had at least one axis that was shorter than the

elevation of the emerged reef (∼1.1 m), the boulder was considered to originate from the emerged reef (i.e., "emerged reef boulders").

To characterize the current velocity of moving boulders along the XDH site, the minimum current velocity (MCV) needed to dislodge and transport boulders were calculated using the following equations (Nandasena et al., 2011).

$$\overset{2}{u} \geq \frac{2(\frac{\rho_s}{\rho_w} - 1)gc(\mu_s \cos\theta + sin\theta)}{C_d(\frac{c}{b}) + \mu_s C_1} \quad (5)$$

(sliding)

$$\overset{2}{u} \geq \frac{2(\frac{\rho_s}{\rho_w} - 1)gc(\cos\theta + (\frac{c}{b})sin\theta)}{C_d(\frac{c^2}{b^2}) + C_1} \quad (6)$$

(rolling)

$$\overset{2}{u} \geq \frac{2(\frac{\rho_s}{\rho_w} - 1)gc\cos\theta}{C_1} \quad (7)$$

(lifting) For a reef-edge boulder in a joint-bounded setting, transport can only be initiated by lifting when u is the current velocity (m/s), C_1 is the lift coefficient (0.178), θ is the angle of bed slope, and μ_s is the coefficient of static friction (0.7).

Coral Age Dating

The U/Th age dating of the youngest surfaces of large boulders helped to determine the deposition time. The U/Th dating analyses were conducted at a multi-collector inductively coupled plasma mass spectrometer (MC-ICPMS) follow a standard procedure performed by Edwards et al. (1987) and Cheng et al. (2013). U/Th ages were calculated using standard equations. We assume that the U/Th age date of the outermost edge of a dead coral head is the time the coral head died (Terry et al., 2016). It is assumed that growing corals were separated from the living reef surface when a boulder was transported from the submerged reef slope and deposited onto the reef flat by high-energy wave events (Yu et al., 2009; Lau et al., 2016). This assumption is supported by previous studies at various sites around the SCS (Zhao et al., 1983; Zhang, 2001; Yu et al., 2012), because "live/dead corals" have been observed presented on the reef slope and fresh coral fragments found were on the reef flat, suggesting living corals have been distributed on the reef slope. The assumption has also been widely validated by the coral dead ages in the top surface of large boulders combining with known historical extreme wave events (e.g., Yu et al., 2012; Lau et al., 2016, 2018). In the study, eight coral samples were collected based on the method of Terry et al. (2016) from the largest 12 boulders for U/Th age dating (**Supplementary Figure 1**). We also collected one oyster shell attached to larger boulders that were above the maximum tide line (**Supplementary Figure 1**) for AMS ^{14}C dating and calibrated using IntCal13 calibration curve (Reimer et al., 2013) with are regional Delt-R of 18 ± 37 (Southon et al., 2002). Therefore, our radiocarbon ages represent minimum dates for boulder dislocation. Our age dating results are listed in **Table 2**.

RESULTS

Boulder Distribution and Morphometry

Figure 2 shows the positions and sizes of measured CBDs at the XDH study site. The fringing reef slopes seaward at an angle of ∼2° (**Figure 1**) and consists of dying, primarily, *Porites* type corals. The slightly emerged reef flat is covered by numerous dead and often inverted *Porites* CBDs with long axes of 0.5–4.0 m (**Figures 2**, **3**). Boulder shapes were platy, sub-angular to rounded, or rectangular to ellipsoidal with some having sharp broken edges (**Figures 2b**, **3b**). The average boulder volume and weight were 0.43 m^3 and 0.78 t, respectively (**Table 3**). The largest and smallest boulder a-axis dimensions were 3.76 and 0.52 m, respectively, while 2.86 and 0.31 m for b-axes, and 2.51 and 0.14 m for c-axes. The estimated range in mass was 0.05– 28.81 t (**Table 3**). The volume of the largest boulder was ∼16 m^3 (0.7 × 3.2 × 2.9 × 2.5 m; **Figure 2c**) with an estimated weight of ∼28.81 t. Approximately 50 and 23% of a-axis orientations of larger boulders (>5 t) were parallel (SW) and perpendicular (NE) to the reef edge, respectively. The orientations of the remaining 27% of larger boulders were SSE, including the three largest boulders observed (**Figure 2**).

Boulders were rarely seen at distances 0–30 m from the reef edge. Approximately 90% of boulders were distributed within the zone of 50–120 m, with a mode at about 82 m from the reef edge (**Figures 2**, **4**). A wide range in boulder weight was also observed from <1 t to >28 t. However, the majority of weights were <2 t, with an estimated mean weight of 0.78 t (**Table 3**). Along the shore, the majority of boulders were distributed on the reef platform, but few large boulders (>1 m) were found in the back-reef moat. Larger boulders were usually found shorter distances to the reef edge (**Figure 4**). The boulder size distribution showed a Gaussian curve (**Figure 3**) as observed in previous studies (Deguara and Gauci, 2017). This indicates that boulders were most likely deposited by one type of wave (**Figure 3**; Barbano et al., 2010), because typhoon wave heights tend to exponentially decrease landward after breaking (Goto et al., 2009, 2010). The negative correlation between boulder size (or weight) and transport distance suggests that the morphology of the coast has great effects on patterns of boulder distribution. The roughness of the uneven reef platform caused by surface pits and detachment scarps inhibits landward transport (Naylor et al., 2016). However, a seaward fining trend (**Figure 4**) was also found at distances from 0–65 m, implying that backwash flow may play a key role in transporting boulders in this zone. Few large boulders at distances >160 m from the reef edge, indicating past high-energy waves that struck Hainan Island, lacked sufficient force to displace boulders (with long axes > 1 m) farther inland (**Figures 2**–**4**). In addition, the carbonate boulders show uneven distribution along with the reef platform and are mostly concentrated in the middle area. This should be mainly related to hydrodynamic field characteristics (e.g., storm energy) and morphology (e.g., reef margin slope) (Wang et al., 2021). Initial terrain modulates the characteristics of the hydrodynamic field and leads to the strengthening of hydrodynamic force in certain areas (Wang et al., 2021).

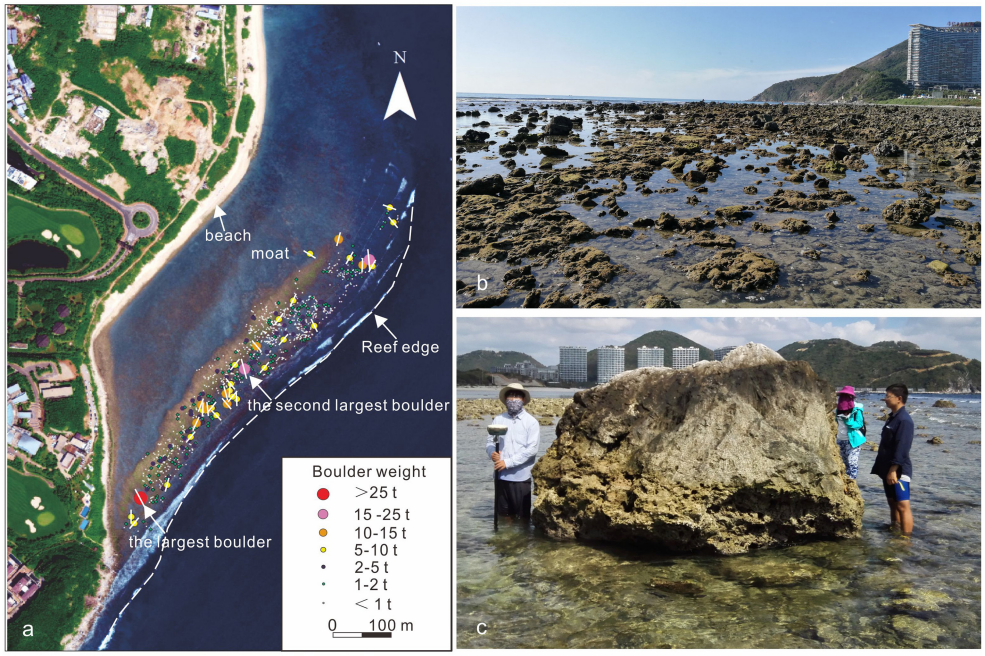

FIGURE 2 | The spatial distribution and morphology of the boulders: **(a)** Google Earth map showing the distribution and weight of boulders at the XDH study site; **(b)** photographs showing the coral boulder field; and **(c)** the largest boulder at the site.

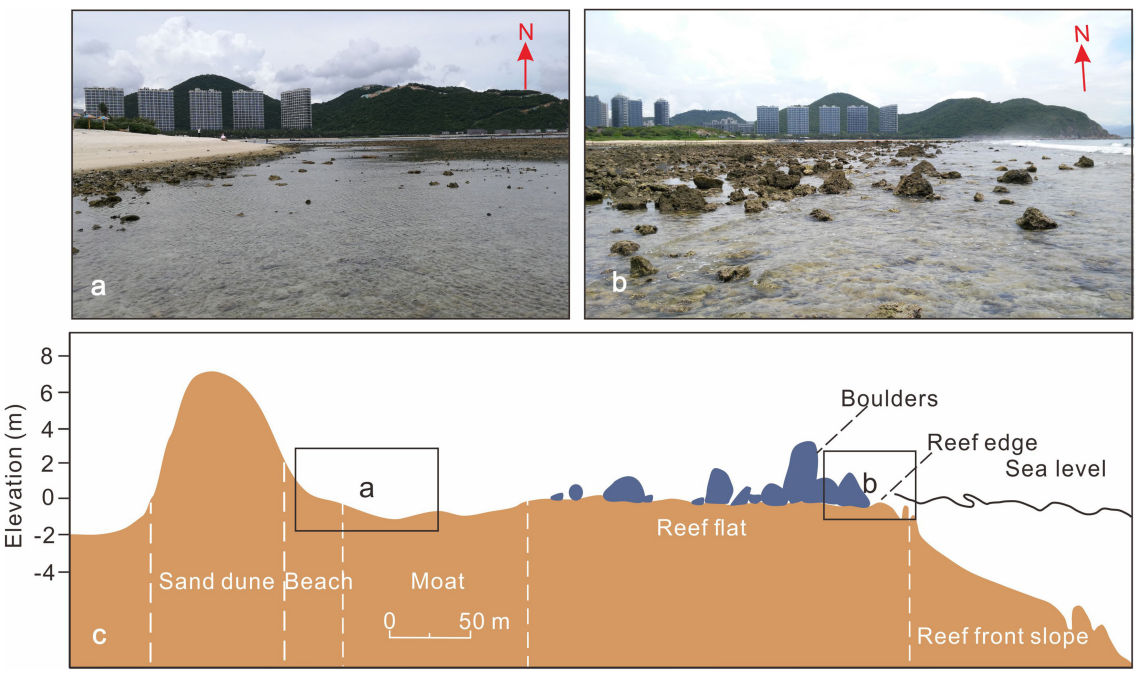

FIGURE 3 | (a) The majority of boulders were deposited 40–140 m from the edge of the reef flat, whereas a few were transported nearer to the beach. **(b)** Carbonate boulders lying near the reef edge. **(c)** The generalized profile and zonation of the XDH study site [modified from Zhang (2001)].

Boulder shape parameters varied significantly at different distances from the reef edge (**Table 4**), falling within various categories (**Figure 5**). As shown in **Table 4**, MPS decreases from 1.91 to 0.91 as the distance from the reef edge increases from 50–80 to 110–150 m. This indicates that the number of spherical boulders gradually diminishes landwards. Clear decreasing trends were similarly found in OPI (0.26 to −0.64) and DRI (0.87 to 0.64) at distances increasing

TABLE 2 | U/Th ages of six large coral boulders on XDH site.

Boulder	^{238}U (ppb)	^{232}Th (ppt)	^{230}Th/^{232}Th	^{230}Th/^{238}U	Corrected ^{230}Th age (yr BP)	Corrected age (CE/BC)
XDH-1001	2430.6 ± 3.0	1581 ±32	74 ± 3	0.0029 ± 0.0001	194 ± 14	1756 ± 14
XDH-933	2065.6 ± 3.3	23035 ± 462	13 ± 0	0.0090 ± 0.0001	514 ± 90	1436 ± 90
XDH-1243	868.1 ± 1.6	4425 ± 89	49 ± 1	0.0151 ± 0.0003	1252 ± 96	698 ± 96
XDH-910	2417.0 ± 5.4	54444 ± 1095	32 ± 1	0.0443 ± 0.0003	3671 ± 258	1721 ± 258
XDH-23	2412.4 ± 2.5	1403 ± 28	576 ± 12	0.0203 ± 0.0001	1872 ± 16	78 ± 16
XDH-24	2556.5 ± 3.5	908 ± 18	928 ± 19	0.0200 ± 0.0001	1842 ± 12	108 ± 12
XDH-748	2341.7 ± 4.8	2417 ± 49	0 ± 1	0.0000 ± 0.0001		Post-1950
XDH-648	2086.5 ± 5.0	729 ± 15	0 ± 6	0.0000 ± 0.0001		Post-1950

All errors are quoted as 2σ.

TABLE 3 | Summary measurements for coastal carbonate boulders on Xiaodonghai (XDH); n = 1,247.

Statistic	Boulder parameter					
	a-axis (m)	b-axis (m)	c-axis (m)	Volume (m^3)	Mass (t)	Elevation (m)
Mean	1.02	0.77	0.52	0.43	0.78	0.21
Standard deviation	0.41	0.29	0.23	1.25	2.28	0.14
Minimum	0.52	0.31	0.14	0.03	0.05	−1.49
Maximimum	3.76	2.86	2.51	15.83	28.81	1.01

from 50–80 to 110–150 m, respectively. This means that the numbers of prolate and disc-shaped boulders increase landwards. This is probably because disc-shaped boulders settle more slowly than other boulder shapes (Flemming, 1964), and are therefore more likely to be carried farther from the reef edge (Wang et al., 2004). Boulder shapes distributed at our XDH study site, therefore, showed a reasonably flat trend.

The Current Velocity Required for Boulder Transport

Figure 6 shows the lower limit of wave-induced current velocities during a typhoon event that can initiate large boulder transport for each transport mode. At the XDH study site, sliding or rolling is considered the most probable transport mode, since 97% of observed boulders were carried <0.5 m above sea level (**Table 3**). This is supported by the numerical results (**Figure 6**), indicating that minimum current velocities (MCVs) of 2.41–5.71, 2.32–5.50, and 4.86–14.74 m/s are sufficient to initiate boulder movement by rolling, sliding, and lifting, respectively. Although some large boulders may be transported by lifting, rolling is considered the most likely mode of transport for the majority of boulders because the elevation of CBDs is almost near the sea level and the inverted orientation of numerous boulders, which satisfies the condition proposed by Terry et al. (2016). Based on our assumption, we determined 2.41–5.71 m/s was the range required to transport these boulders (**Figure 6**; **Table 5**). In particular, boulders may be moved step by step in a series of many waves during typhoons, with estimated velocities representing the minimum current velocities experienced.

Ages Dating and Comparison With Historical Typhoon Records

The nine ages of the 12 largest CBDs (**Tables 2**, **3**) range from 1721 BC to AD 1756 (except modern age samples), with accumulated age uncertainties typically varying between 0.6 and 15% of the absolute age. Five samples were dated within the last 2,000 years, with four young boulders dated to the last 1,000 years. The earliest documented large wave events on Hainan Island can be traced back to AD 982. This allows us to compare historical and geological records over the past millennium. The age of XDH-1001 (AD 1756 ± 14) may correspond to large typhoon events in AD 1751/1753 (**Table 2**). The devastating typhoon of 1751 is recognized as causing one of the worst floods on the east coast of Hainan Island. Descriptions record that "*Strong wind, powerful waves overflow onto the shore and Wanning city was flooded, numerous people died*" (Chen, 1995). Similarly, the severe typhoon of 1753 was also extremely violent, producing strong waves that swept across Hainan Island, especially in the south (Chen, 1995). Descriptions record the following conditions: "*Extraordinarily strong winds and rainstorm, typhoon flood onto the village, hundreds of great trees and crops blow down in Sanya city; more that 50% houses destroyed, 27 people were drowned by typhoon flood in Wanning city; buildings destroyed, trees and crops all broken, in Haikou city.*" The age of XDH-933 (AD 1436 ± 90) may correspond to the catastrophic typhoon of AD 1524 (**Table 2**). The typhoon ravaged the southeast coast of Hainan Island and is considered the greatest calamity during the Ming dynasty (Chen, 1995). The description records that "*In August, extraordinarily strong wind and rainstorm, typhoon floods over the land for a distance of more than 10 km, several ships washed up on land more than 1 km, more*

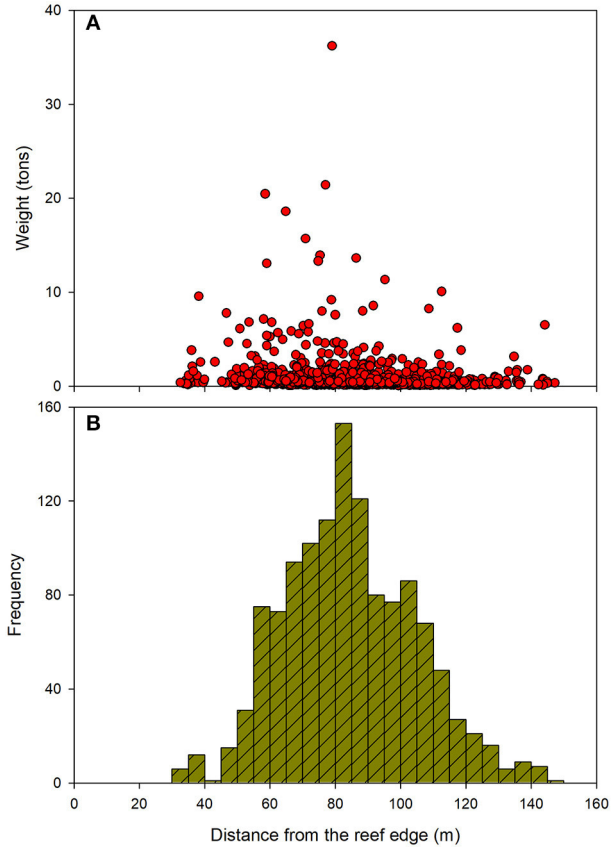

FIGURE 4 | The distribution of boulder weights **(A)** and the number of boulders **(B)** on the coast according to the distance from the reef edge.

than 80% houses destroyed, countless livestock and people were drowned, never seen or heard of before by old people in Wanning city" (Chen, 1995). Given the errors on the U/Th dating results, the large typhoon in AD 1524 is consistent with our measured boulder ages. Moreover, some large boulders have been moved by modern typhoons according to the survey of local residents, such as the No. 648 boulder was deposited during landfalling typhoon Pamela over the Hainan Island in 1972 CE. This result was also consistent with the No. 648 boulder U/Th age.

Identification of Paleo-Typhoon Events

Table 3 shows that the largest boulder detached from the reef edge had an estimated mass of 28.81 t. As specific signatures have not yet been developed to differentiate categorically between typhoon and tsunami boulders, it is important to adopt multiple factors (e.g., coastal geomorphology, boulders spatial distribution, and history of typhoon activities) to determine the reliability of typhoon reason (Goto et al., 2010; Cox et al., 2012; Nakamura et al., 2014; Lau et al., 2016). Previous investigations showed that maximum boulder weights displaced from the reef edge by typhoon flood inundation are usually $\leq$100 t (Goto et al., 2009), although more recent studies have identified larger transported clasts up to $\sim$200 t (May et al., 2015). These numerous data indicate that typhoon flood inundation plays a significant role in producing boulder deposits in the region.

Morphometric investigations show that carbonate boulders with different sizes have been transported at varying distances from the reef edge (**Figures 2a**, **4**). An inverse pattern between boulder size and transport distance has been identified at our XDH study site (**Figure 4**), a type of distribution often observed elsewhere (Goto et al., 2009, 2010; Deguara and Gauci, 2017) and associated with typhoon wave deposits (Goto et al., 2010). Goto et al. (2010) and Barbano et al. (2010) suggested that boulder distributions following multiple Gaussian curves, rather than falling into a single group, would be associated with different types of waves. Thus, the single distribution at our XDH site is evidence for one wave type. The flat trend of the boulder distribution (**Table 4**) might also be produced by a single wave type. Furthermore, the predominant SSW to WSW alignment of long axis orientations for larger boulders (>5 t) (**Figure 2**) is consistent with the strong impact of typhoon waves reaching the shoreline (State Oceanic Administration, 1999). In addition, the observed landward-fining trend of boulders sizes (**Figures 3**, **4**) requires the action of multiple waves (Goto et al., 2009; Deguara and Gauci, 2017), indicating that coastlines of the study region have been exposed to frequent high-energy events. Taking all these morphometric characteristics into consideration, we reasonably think that typhoon events are responsible for the spatial distribution of boulders. This is also supported by the result of analyzing the theoretical distribution pattern of storm boulders on the XDH site (Wang et al., 2021). In addition, there are few historical records of tsunamis on the Hainan Island coastline compared with the northern South China Sea (Liu et al., 2007; Mak and Chan, 2007). In addition, the measured dates of large CBDs during the past 1,000 years are all consistent with historical catastrophic typhoons (**Table 2**; Chen, 1995; above section). Furthermore, the only observed tsunami event occurred on January 4, 1992, generated by an Mw3.7 earthquake offshore from southwestern Hainan. The maximum tsunami wave recorded in Yulin Bay was only 0.78 m high (Ye et al., 1994).

Numerical models of current velocity indicate that MCVs of 2.41–5.71 m/s are required to transport the observed boulders (**Figure 6**). Similarly, on Lanyu Island off southern Taiwan, Nakamura et al. (2014) calculated MCVs of 1.4–16.9 m/s for CBDs found at distances up to 120 m from the shore. In comparison, investigations of transported carbonate boulders on Ko Larn Island in southern Thailand by Terry et al. (2015) showed that boulder transport occurred at MCVs of 2.7–7.1 m/s, whereas CBDs carried up to 4.7 m above mean sea level on Ko Samui Island indicate past MCVs of 2.3–8.6 m/s (Terry et al., 2016). In the Philippines, Kennedy et al. (2017) revealed how the passage of Super Typhoon Haiyan in 2013 produced extreme high-energy waves that were able to displace a giant boulder of volume 83 m^3 and mass 208 t, the transport of which required MCVs up to 8.9–9.6 m/s (May et al., 2015). Our MCV calculations from carbonate boulder deposits at XDH are therefore consistent with data from other typhoon-impacted coastlines across tropical Asia–Pacific region. Combining such evidence, it appears that the accumulation of carbonate boulders at our XDH site is the result of high-energy large typhoons.

TABLE 4 | Shape parameters and standard deviations (SD) of carbonate boulders.

Distance (m)	Number of boulders	MPS		DRI		OPI	
		Average	SD	Average	SD	Average	SD
0–50	40	0.70	0.14	0.52	0.40	−0.33	7.42
50–80	487	1.19	0.19	0.87	0.74	0.26	11.54
80–110	585	0.93	0.17	0.66	0.47	−0.29	9.23
110–150	135	0.91	0.17	0.64	0.41	−0.64	8.35

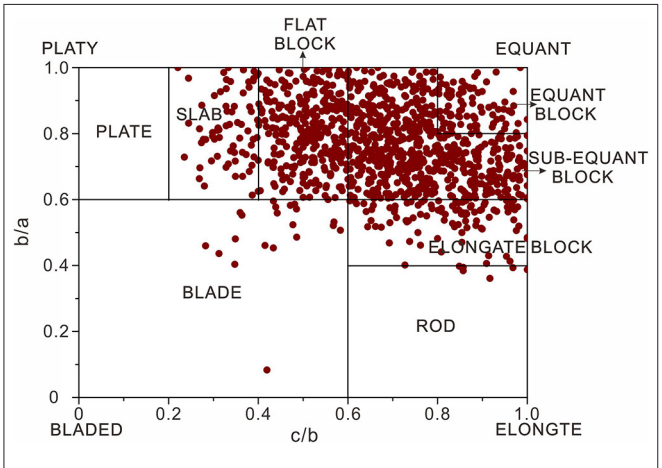

FIGURE 5 | Coral boulder shapes at the XDH study site plotted on a Zingg diagram (Zingg, 1935; Blott and Pye, 2010; Terry et al., 2015).

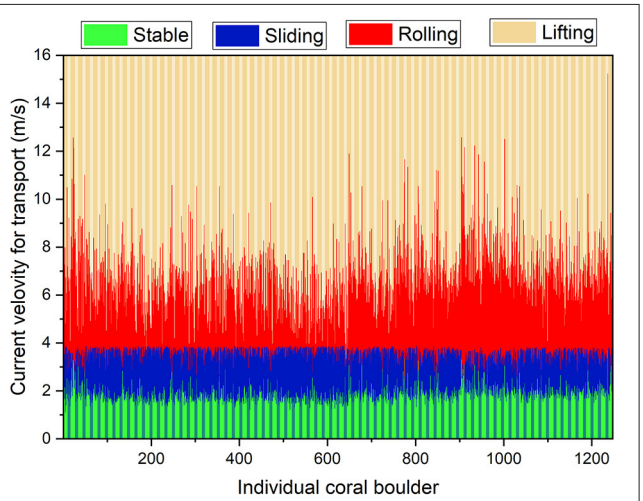

FIGURE 6 | Current velocities for initiation of boulders transport by different transport modes.

DISCUSSION

Large Typhoon Spatial Variation in Coast SCS and Western North Pacific

Coral boulders provide key insight into the relationship between basin-wide large typhoon activity and paleoclimate change (**Figure 7**). The relationship between boulder ages and paleoclimate variability may be revealed by examining the records from different sites. In combination with the previous findings (Zhou et al., 2019b), we propose that there have been seven major periods of large typhoon periods (T1–T7) on the coast of Hainan Island (**Figure 7**), i.e., 1800–1500 BCE (T7), 1200–900 BCE (T6), 50–120 CE (T5), 550-800 CE (T4), 900-1,000 CE (T3), 1350–1900 CE (T2), and 1910–2000 CE (T1).

In the northwestern Pacific and South China Sea regions, modern observations and paleotempestological studies suggest that ENSO plays a significant role in typhoon longitudinal variations, with more movement routes directed toward Korea and Japan during El Niño times, but toward the northern South China Sea during La Niña times (Chan, 1985, 2005; Woodruff et al., 2009; Chen et al., 2012; Zhou et al., 2019a,b). However, little is known about the relationship between the major typhoon activities and climate dynamics at centennial-millennial scales. Comparisons between the patterns of the two routes suggest a general inverse correlation (**Figures 7A,C,D**). For example, the seven periods with intense, frequent typhoons in Hainan Island (T1–T7) match the periods of more La Niña-like times at centennial-millennial scales. In contrast, more active typhoons in Japan and Korea (except T3 and T7) occur mainly during El Niño times (Woodruff et al., 2009; Yang et al., 2017; **Figures 7A,H**). This confirms that the longitudinal variations of the intense typhoons are mainly regulated by ENSO patterns over the past 4,000 years (Zhou et al., 2019b).

However, two intense typhoon periods (T4 and T6) do not follow the pattern of ENSO, indicating that other climate drivers may be involved. Previous studies and modern observations both suggest that TCs variations in the WNP and SCS also greatly regulated by the thermal state of the western Pacific warm pool (WPWP) (Yue et al., 2019; Zhou et al., 2019a,b). **Figures 7C,H** show that almost all typhoon periods in the SCS match the warmer WPWP. This correlation between intense typhoon periods and warm sea surface temperature (SST) of WPWP phases has been observed by modern observations (Chen and Huang, 2008). During the warmer years of the WPWP, more TCs would be formed in the western part of WNP, facilitating TCs landfall in the SCS (Chen and Huang, 2008).

It should be noted that the increased typhoon activity occurred both in the northern SCS and eastern WNP (Korea, Japan, East China Sea) during the period of T3 and T7, suggesting that intense typhoon activity in the SCS and WNP should involve other climatic factors (**Figures 7A,C**). Observation records indicate that the active phase (northward) of Intertropical

TABLE 5 | Results from hydrodynamic equations showing the calculated minimum velocities capable of moving the largest 12 boulders.

Boulder number	Axis length (m)	Velocity (m/s)	Axis length (m)	Velocity (m/s)	Axis length (m)	Velocity (m/s)
	a	b	c	Sliding	Rolling	Lifting
XDH-933	2.67	2.01	1.62	3.71	4.72	11.83
XDH-942	3.31	1.69	1.52	3.41	4.16	11.46
XDH-1001	2.51	1.96	1.69	3.67	4.55	12.08
XDH-903	2.44	2.35	1.71	3.99	5.27	12.15
XDH-910	2.51	2.03	1.60	3.72	4.77	11.76
XDH-24	3.51	2.08	1.59	3.36	4.88	11.72
XDH-23	3.27	2.29	1.71	3.94	5.16	12.14
XDH-1235	3.15	2.86	2.51	4.44	5.46	14.73
XDH-1243	2.44	2.33	1.20	3.61	5.65	10.18
XDH-648	2.30	2.01	1.53	3.70	4.80	11.50
XDH-748	2.32	2.06	1.20	3.69	5.24	10.18
XDH-774	3.76	2.42	1.47	4.01	5.62	11.27

Convergence Zone (ITCZ) in the WNP could generate more TCs than that of inactive phases (southward) in the WNP (Ma and Chen, 2009; Cao et al., 2012). Therefore, it is hypothesized that more or less TCs and more northerly or southerly TCs genesis location likely leads to more typhoons move to both the northern and southern Northwestern Pacific during the strength ITCZ (weak ITCZ), respectively, as indicated by Chen et al. (2019). The multi-sites in the SCS and WNP over the past 1,500 years provide us the opportunity to test the role of ITCZ in governing latitudinal large typhoon activity in the centennial to millennial time-scale (**Figure 7**). Comparisons of the large typhoon proxy records generally support the hypothesis model between Northern WNP (the regions of Korea, Japan, and the East China Sea) and Southern WNP (Hainan Island, Taiwan Island, southern SCS, and Thailand) in typhoon activity over the past 1,500 years. Increased typhoon intensity observed in coastal of northern WNP (Korea; East China Sea; **Figures 7A–F**) and southern WNP during the T3 and T7 periods generally match the strength (northward) ITCZ. In contrast, the relative quiescence conditions in Northern WNP (**Figures 7A,B**; Korea; Japan; East China Sea) during the T2, T4, and T6 periods match the period of increased large typhoons at the southern WNP (Hainan Island; Taiwan Island; SCS and Thailand Gulf; **Figures 7C–F**), with the weak (southward) ITCZ phases. Historical records from the eastern coast of Asia also support an ITCZ-driven inverse typhoon activity pattern in WNP (Chen et al., 2019). Thus, similar to observations and historical studies (Cao et al., 2012; Chen et al., 2019), the CBD records from the XDH site support the pattern of more large typhoons move to Hainan Island during weak ITCZ phases. However, frequent large typhoons north move to the East China Sea during the weak ITCZ phase (T1), which should be associated with the thermal state of Kuroshio current. Because of the warmer SST of Kuroshio current (Cai et al., 2012) post 1900, it may have strengthened the intensity of TCs when TCs in the East China Sea pass over the Kuroshio (Yu et al., 2019).

Future Typhoon Risk of the Southern Coast of Hainan Island

Our findings from carbonate boulder deposits at Xiaodonghai provide evidence of the potential hazard exposure to extreme typhoon events in this area and surrounding low-lying coasts. Frequent incidences of people and infrastructure being inundated by large typhoon events are known on Hainan Island over the past 1,000 years (Chen, 1995). In southern Hainan, the rapid development of coastal tourism since the late 20th century has greatly promoted the aggregation of a large number of facilities in low-lying coastal areas and the extension of small fishing villages. Now the resident population (e.g., in the Sanya city) is about 15 times larger than that of 1750 and dramatically increased since the 1970s (Hainan Procincial Bureau of Statistics, 1992). With the development of Hainan Island, new infrastructure (e.g., harbors) and the number of residential and commercial buildings facing the threat of inundation is growing considerably. Instrumental records show that the ITCZ position has a gradually equatorward movement since 1949 CE (Ma and Chen, 2009), which means that more TCs would be a movement to the southern WNP, especially the northern SCS (Hainan Island). Moreover, the warm state of the WPWP will strengthen the SST of the WNP and SCS with future global warming, and so the north expanded warmer SST of WPWP is to guide more intense typhoons toward Hainan Island (**Figures 7C,G**; Yue et al., 2019; Zhou et al., 2019b). Furthermore, the risk of catastrophic typhoons will increase in the future according to the sea-level rise predictions of global climate models (IPCC, 2012). Our results indicate that the storm boulder records can be used to obtain information on typhoon intensity and frequency and to examine the projections of future large typhoons under changing climate.

CONCLUSIONS

Carbonate boulder deposits at the XDH study site on southern coastal Hainan Island, China, provide evidence of

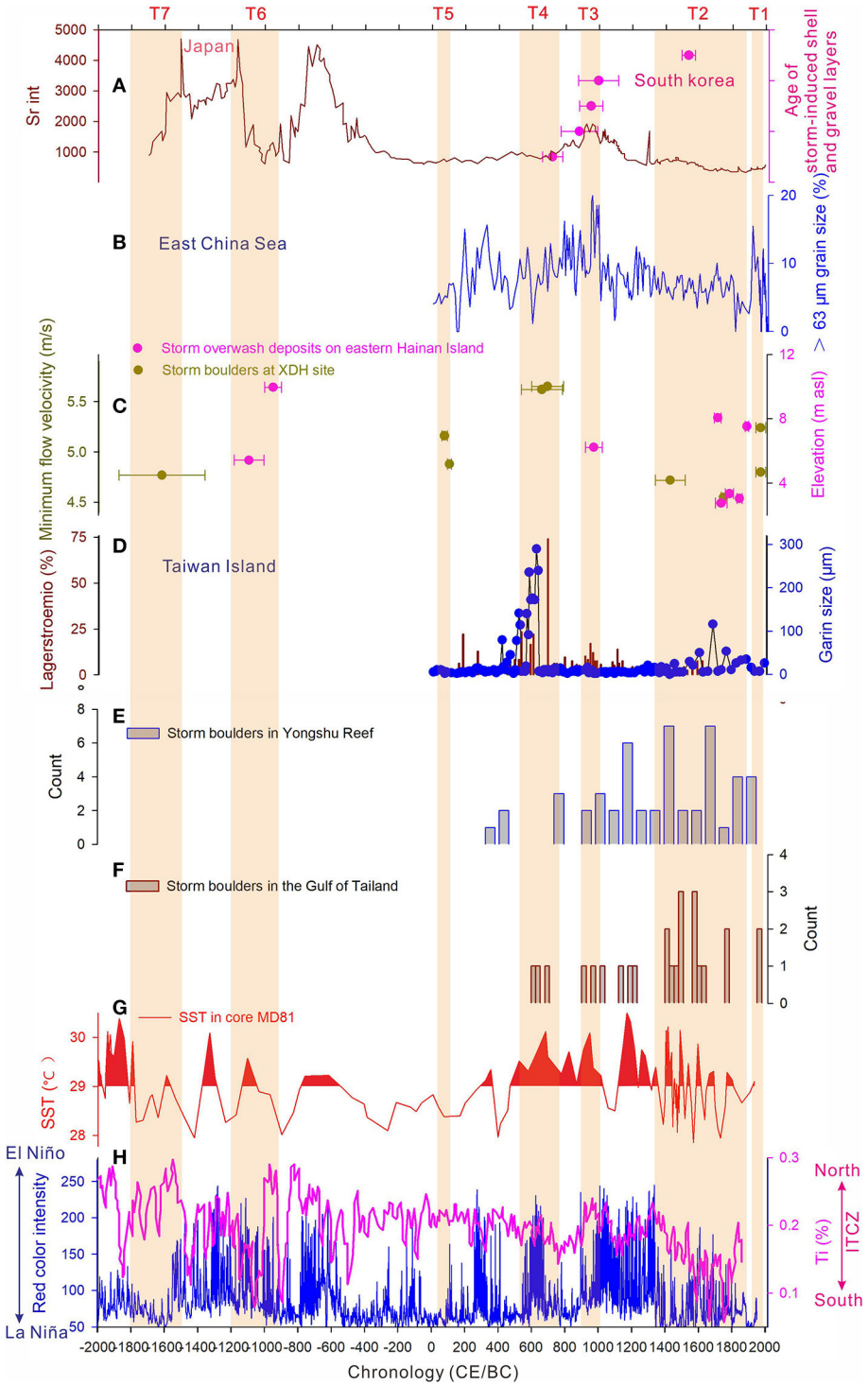

FIGURE 7 | Comparison of the large typhoon periods on Hainan Island with regional paleo-typhoon reconstructions from the SCS and WNP. **(A)** The paleo-typhoon reconstructions from the Kamikoshiki Island, Japan (Woodruff et al., 2009) and large typhoon induced shell layers deposits (Yang et al., 2017); **(B)** typhoon-induced coarse grain deposits from East China Sea (Zhou X. et al., 2019); **(C)** large typhoon periods in the Hainan Island (this study; Zhou et al., 2019b); **(D)** sedimentary records of large typhoon-induced extreme rainfall events from Taiwan Island (Chen et al., 2012); **(E)** Storm boulder deposits from Yongshu Reef, SCS **(E)** and Tailand **(F)**; **(G)** SST reconstruction from core MD-81 (Stott et al., 2004); **(H)** El-Niño frequency reconstruction from Laguna Pallcacocha, Ecuador (Moy et al., 2002) and ITCZ reconstruction from anoxic Cariaco Basin (Haug et al., 2001). The brown bars representing large typhoon periods.

high-energy large typhoon events. A morphometric analysis of observed boulders at the XDH site revealed a Gaussian curve distribution, suggesting that boulders were most likely deposited by a single wave type. The application of hydrodynamic equations showed that the boulders could have been transported initially by a maximum current velocity of 5.71 m/s. These results are consistent with local observations and with findings from other coastlines in the Asia–Pacific region that periodically experience direct hits by large typhoons.

Comparison of CBD U/Th ages with historical records suggests that two large boulders (XDH-1001 and XDH-933) were probably detached onto the reef flat by devastating typhoons that occurred in October 1751 (or September 1753), and August 1524, respectively. There is no instrumental or historical evidence of a tsunami capable of transporting these boulders. In contrast, there is adequate evidence of historical extreme typhoons large enough to displace the boulders. Based on our analysis, we argue that only an exceptionally strong unknown typhoon could have transported and emplaced all the boulders. Together with previous large typhoon records, seven large typhoon periods occurred in 1800–1500 BCE (T7), 1200–900 BCE (T6), 50–120 CE (T5), 550–800 CE (T4), 900–1000CE (T3), 1350–1900CE (T2), and 1910–2000 CE (T1) on the coast of Hainan Island. After comparison with regional proxies, we found that the spatiotemporal change of large typhoons in the SCS and WNP was significantly controlled by ENSO (east-west shift), WPWP, and ITCZ (south-north movement) activities.

This paper highlights the potential risk of a large typhoon on the heavily populated and rapidly economic developing southern coast of Hainan Island. The vulnerability of this area should be considered in coastal risk assessment.

DATA AVAILABILITY STATEMENT

The original contributions presented in the study are included in the article/**Supplementary Material**, further inquiries can be directed to the corresponding author.

AUTHOR CONTRIBUTIONS

LZ designed the research, analyzed the data, and wrote the manuscript. SG guided the whole study and revised the manuscript. JJ and YY helped to revise the manuscript and the result analyses. CT and AW revised the manuscript and gave comments. All authors contributed to the article and approved the submitted version.

FUNDING

This work was funded by grants from the Natural Science Foundation of China (Nos. 41706096 and 41530962) and the Priority Academic Program Development of Jiangsu Higher Education Institutions and supported by the Research Start-up Project of Jiangsu Normal University (19XSRX006); Opening Foundation of Hainan Key Laboratory of Marine Geological Resources and Environment (HNHYDZZYHJKF005); the High-level Talent Program of Basic and Applied Basic Research Programs (Field of Natural Science) in Hainan Province (No. 2019RC349).

SUPPLEMENTARY MATERIAL

The Supplementary Material for this article can be found online at: https://www.frontiersin.org/articles/10.3389/fmars.2021.746773/full#supplementary-material

REFERENCES

Banerjee, D., Murray, A. S., and Foster, I. D. L. (2001). Scilly Isles, UK: optical dating of a possible tsunami deposit from the (1755). Lisbon earthquake. *Quat. Sci. Rev.* 20, 715–718. doi: 10.1016/S0277-3791(00)00042-1

Barbano, M. S., Pirrotta,. C., and Gerardi,. F. (2010). Large boulders along the south-eastern Ionian coast of Sicily: storm or tsunami deposits? *Mar. Geol.* 275, 140–154. doi: 10.1016/j.margeo.2010.05.005

Blott, S. J., and Pye, K. (2010). Particle shape: a review and new methods of characterization and classification. *Sedimentology* 55: 31–63. doi: 10.1111/j.1365-3091.2007.00892.x

Cai, W., Zhang, L., Nakamura, H., Timmermann, A., and Wu, L. (2012). Enhanced warming over the global subtropical western boundary currents. *Nat. Clim. Change* 2, 161–166. doi: 10.1038/nclimate1353

Cao, X., Huang, P., Chen, G., and Chen, W. (2012). Modulation of western North Pacific tropical cyclone genesis by intra-seasonal oscillation of the ITCZ: A statistical analysis. *Adv. Atmos. Sci.* 29, 744–754. doi: 10.1007/s00376-012-1121-0

Chan, J. (2005). Interannual and interdecadal variations of tropical cyclone activity over the western north pacific. *Meteorol. Atmos. Phys.* 89, 143–152. doi: 10.1007/s00703-005-0126-y

Chan, J. C. L. (1985). Tropical cyclone activity in the northwest pacific in relation to the El Niño/Southern oscillation phenomenon. *Mon. Wea. Rev.* 113, 599–606. doi: 10.1175/1520-0493(1985)113<0599:tcaitn>2.0.co;2

Chen, B., Chen, Z., Stephenson, W., and Finlayson, B. (2011). Morphodynamics of a boulder beach, Putuo Island, SE China coast: the role of storms and typhoon. *Mar. Geol.* 283, 106–115. doi: 10.1016/j.margeo.2010.10.004

Chen, G., and Huang, R. (2008). Influence of monsoon over the warm pool on interannual variation on tropical cyclone activity over the western north pacific. *Polit. Stud. Rev.* 11, 319–328. doi: 10.1007/s00376-008-0319-7

Chen, H. F., Liu, Y. C., Chiang, C. W., Liu, X., Chou, Y. M., and Pan, H. J. (2019). China's historical record when searching for tropical cyclones corresponding to intertropical convergence zone (ITCZ) shifts over the past 2 kyr. *Clim. Past.* 15, 279–289. doi: 10.5194/cp-15-279-2019

Chen, H. F., Wen, S. Y., Song, S. R., Yang, T. N., Lee, T. Q., Lin, S. F., et al. (2012). Strengthening of paleo-typhoon and autumn rainfall in taiwan corresponding to the southern oscillation at late holocene. *J. Q. Sci.* 27, 964–972. doi: 10.1002/jqs.2590

Chen, H. S. (1995). *Natural disasters in Hainan province during the past (1000) Years (in Chinese)*. Haikou: Hainan Press.

Cheng, H., Edwards, R. L., Shen, C. C., Polyak, V. J., Asmerom, Y., Woodhead, J., et al. (2013). Improvements in ^{230}Th dating, ^{230}Th and ^{234}U half-life values, and U–Th isotopic measurements by multi-collector inductively coupled plasma mass spectrometry. *Earth Planet. Sci. Lett.* 371, 82–91. doi: 10.1016/j.epsl.2013.04.006

Cox, R., Zentner, D. B., Kirchner, B. J., and Cook, M. S. (2012). Boulder ridges on the Aran Islands (Ireland): recent movements caused by storm waves, not tsunamis. *J. Geol.* 120, 249–272. doi: 10.1086/664787

Deguara, J. C., and Gauci, R. (2017). Evidence of extreme wave events from boulder deposits on the south-east coast of Malta (Central Mediterranean). *Nat. Hazards* 86, 543–568. doi: 10.1007/s11069-016-2525-4

Dobkins Jr., J. E., and Folk, R. L. (1970). Shape development on Tahiti-nui. *J. Sediment. Res.* 40, 1167–1202. doi: 10.1306/74D72162-2B21-11D7-8648000102C1865D

Edwards, R. L., Chen, J. H., and Wasserburg, G. J. (1987). $^{238}U^{234}U^{230}Th^{232}Th$ systematics and the precise measurement of time over the past 500,000 years. *Earth Planet. Sci. Lett.* 81, 175–192. doi: 10.1016/0012-821X(87)90154-3

Etienne, S. (2012). Marine inundation hazards in French Polynesia: geomorphic impacts of Tropical Cyclone Oli in February 2010. *Geol. Soc. Lond.* 361, 21–39. doi: 10.1144/SP361.4

Flemming, N. C. (1964). Tank experiments on the sorting of beach material during cusp formation. *J. Sediment. Res.* 34, 112–122. doi: 10.1306/74D70FE2-2B21-11D7-8648000102C1865D

Goff, J., Dudley, W. C., Cain, G., and Coney, J. P. (2006). The largest local tsunami in 20th century Hawaii. *Mar. Geol.* 226, 65–79. doi: 10.1016/j.margeo.2005.09.017

Gönnert, G., and Birgit, G. (2015). A multi-method approach to develop extreme storm surge events to strengthen the resilience of highly vulnerable coastal areas. *Coast. Eng. J.* 57:1540002. doi: 10.1142/S0578563415400021

Goto, K., Okada, K., and Imamura, F. (2009). Characteristics and hydrodynamics of boulders transported by storm waves at Kudaka Island, Japan. *Mar. Geol.* 262, 14–24. doi: 10.1016/j.margeo.2009.03.001

Goto, K., Okada, K., and Imamura, F. (2010). Numerical analysis of boulder transport by the 2004 Indian Ocean tsunami at Pakarang Cape, Thailand. *Mar. Geol.* 268, 97–105. doi: 10.1016/j.margeo.2009.10.023

Hainan Procincial Bureau of Statistics. (1992). Beijing: Chinese Statistic Press, 94–137.

Haug, G. H., Hughen, K. A., Sigman, D. M., Peterson, L. C., and Röhl, U. (2001). Southward migration of the Intertropical Convergence Zone through the Holocene. *Nature* 293, 1304–1308. doi: 10.1126/science.1059725

Illenberger, W. K. (1991). Pebble shape (and size). *J. Sediment. Res.* 61, 756–767. doi: 10.1306/D42677C6-2B26-11D7-8648000102C1865D

Imamura, F., Goto, K., and Ohkubo, S. (2008). A numerical model for the transport of a boulder by tsunami. *J. Geophys. Res.* 113:C011008. doi: 10.1029/2007JC004170

IPCC (2012). "Managing the risks of extreme events and disasters to advance climate change adaptation," in *A Special Report of Working Groups Iand II of the Intergovernmental Panel on Climate Change*, eds C. B. Field, V. Barros, T. F. Stocker, D. Qin, D. J. Dokken, K. L. Ebi, et al. (Cambridge, NewYork, NY: Cambridge University Press). p. 1–324.

Kennedy, A. B., Mori, N., Yasuda, T., Shimozono, T., Tomiczek, T., Donahue, A., et al. (2017). Extreme block and boulder transport along a cliffed coastline (Calicoan Island, Philippines) during Super Typhoon Haiyan. *Mar. Geol.* 383, 65–77. doi: 10.1016/j.margeo.2016.11.004

Kitamura, A., Imai, T., Miyairi, Y., Yokoyama, Y., and Iryu, Y. (2017). Radiocarbon dating of coastal boulders from kouzushima and miyake islands off tokyo metropolitan area, Japan: implications for coastal hazard risk. *Quatern. Int.* 456, 28–38. doi: 10.1016/j.quaint.2017.05.040

Lau, A. A., Terry, J. P., Ziegler, A., Pratap, A., and Harris, D. (2018). Boulder emplacement and remobilisation by cyclone and submarine landslide tsunami waves near Suva City, Fiji. *Sediment. Geol.* 364, 242–257. doi: 10.1016/j.sedgeo.2017.12.017

Lau, A. A., Terry, J. P., Ziegler, A. D., Switzer, A., D., Lee, Y. (2016). Understanding the history of extreme wave events in the Tuamotu Archipelago of French Polynesia from large carbonate boulders on Makemo Atoll, with implications for future threats in the central South Pacific. *Mar Geol.* 380, 174–190. doi: 10.1016/j.margeo.2016.04.018

Liu, Y., Santos, A., Wang, S. M., Shi, Y., Liu, H., and Yuen, D. A. (2007). Tsunami hazards along Chinese coast from potential earthquakes in South China Sea. *Phys. Earth. Planet. Int.* 163, 233–244. doi: 10.1016/j.pepi.2007.02.012

Lorang, M. S. (2011). A wave-competence approach to distinguish between boulder and megaclast deposits due to storm waves versus tsunamis. *Mar. Geol.* 283, 90–97. doi: 10.1016/j.margeo.2010.10.005

Ma, L. P., and Chen, L. S. (2009). The relationship between global warming and the variation in tropical cyclone frequency over the Western North Pacific. *J. Trop. Meteorol.* 15, 38–44.

Mak, S., and Chan, L. S. (2007). Historical tsunamis in south China. *Nat Hazard.* 43, 147–164. doi: 10.1007/s11069-007-9113-6

May, S. M., Engel, M., Brill, D., Cuadra, C., Lagmay, A. M. F., Santiago, J., et al. (2015). Block and boulder transport in eastern Samar (Philippines) during Supertyphoon Haiyan. *Earth. Surf. Dyn.* 3, 543–558. doi: 10.5194/esurf-3-543-2015

Moy, C. M., Seltzer, G. O., Rodbell, D. T., and Anderson, D. M. (2002). Variability of ElNino/Southern oscillation activity at millennial timescales during the Holocene epoch. *Nature* 420, 162–165. doi: 10.1038/nature01194

Nadin, R., Sarah, O., and Xu, Y. L. (2016). *Climate Risk and Resilience in China*. London: Routledge: Taylor and Francis Group.

Nakamura, M., Arashiro, Y., and Shiga, S. (2014). Numerical simulations to account for boulder movements on Lanyu Island, Taiwan: tsunami or storm? *Earth Planets Space* 66, 1–20. doi: 10.1186/1880-5981-66-128

Nandasena, N. A. K., Paris, R., and Tanaka, N. (2011). Reassessment of hydrodynamic equations: minimum current velocity to initiate boulder transport by high energy events (storms, tsunamis). *Mar. Geol.* 281, 70–84. doi: 10.1016/j.margeo.2011.02.005

Nandasena, N. A. K., Tanaka, N., Sasaki, Y., and Osada, M. (2013). Boulder transport by the 2011 Great East Japan tsunami: comprehensive field observations and whither model predictions? *Mar. Geol.* 346, 292–309. doi: 10.1016/j.margeo.2013.09.015

Naylor, L. A., Stephenson, W. J., Smith, H., Way, O., Mendelssohn, J., and Cowley, A. (2016). Geomorphological control on boulder transport and coastal erosion before, during and after an extreme extra-tropical cyclone. *Earth. Surf. Proc. Land.* 41, 685–700. doi: 10.1002/esp.3900

Nott, J. (1997). Extremely high-energy wave deposits inside the Great Barrier Reef, Australia: determining the cause—tsunami or tropical cyclone. *Mar. Geol.* 141, 193–207. doi: 10.1016/S0025-3227(97)00063-7

Nott, J. (2000). Records of prehistoric tsunamis from boulder deposits–evidence from Australia. *Sci. Tsunami Hazards.* 18, 3–14.

Nott, J. (2003). Waves, coastal boulder deposits and the importance of pre-transport setting. *Earth Planet. Sci. Lett.* 210, 269–276. doi: 10.1016/S0012-821X(03)00104-3

Paris, R., Naylor, L. A., and Stephenson, W. J. (2011). Boulders as a signature of storms on rock coasts. *Mar. Geol.* 283, 1–11. doi: 10.1016/j.margeo.2011.03.016

Pettijohn, F. J., Potter, P. E., and Siever, R. (1987). *Sand and Sandstone*. New York, NY: Springer Verlag.

Reimer, P. J., Bard, E., Bayliss, A., Beck, J. W., and Staff, R. A. (2013). Intcal13 and marine13 radiocarbon age calibration curves 0-50,000 years cal BP. *Radiocarbon* 55, 1869–1887. doi: 10.2458/azu_js_rc.55.16947

Sneed, E. D., and Folk, R. L. (1958). Pebbles in the lower Colonado River, Texas, a study in particle morphogenesis. *J. Geol.* 66, 114–150. doi: 10.2307/30058239

Southon, J., Kashgarian, M., Fontugne, M., Metivier, B., and Yim, W. W. S. (2002). Marine reservoir corrections for the Indian Ocean and Southeast Asia. *Radiocarbon* 44, 167–180. doi: 10.1017/S0033822200064778

State Oceanic Administration (1999). *Records of China Bays 11th Fascicule—The Bays in Hainan Province (in Chinese)*. Beijing: China Ocean Press, 89–108.

Stott, L. D., Cannariato, K. G., Thunell, R., Haug, G. H., Koutavas, A., and Lund, S. (2004). Decline of surface temperature and salinity in the western tropical Pacific Ocean in the Holocene epoch. *Nature* 431, 56–59. doi: 10.1038/nature02903

Suursaar, Ü., Jaagus, J., and Tõnisson, H. (2015). How to quantify long-term changes in coastal sea storminess? *Estuar. Coast. Shelf Sci.* 156, 31–41. doi: 10.1016/j.ecss.2014.08.001

Terry, J. P., Dunne, K., and Jankaew, K. (2016). Prehistorical frequency of highes in coastal sea stotion events driven by typhoons in the Bay of Bangkok (Thailand), interpreted from coastal carbonate boulders. *Earth. Surf. Proc. Land.* 41, 553–562. doi: 10.1002/esp.3873

Terry, J. P., Goff, J., and Jankaew, K. (2018). Major typhoon phases in the upper gulf of thailand over the last 1.5 millennia, determined from coastal deposits on rock islands. *Quatern. Int.* 487, 87–98. doi: 10.1016/j.quaint.2018.04.022

Terry, J. P., Jankaew, K., and Dunne, K. (2015). Coastal vulnerability to typhoon inundation in the Bay of Bangkok, Thailand? evidence from carbonate boulder deposits on Ko Larn Island. *Estuar. Coast. Shelf Sci.* 165, 261–269. doi: 10.1016/j.ecss.2015.05.028

Von Storch, H., and Reichardt, H. (1997). A scenario of storm surge statistics for the german bight at the expected time of doubled atmospheric carbon dioxide concentration. *J. Clim*. 10, 2653–2662.

Vousdoukas, M. I., Voukouvalas, E., Annunziato, A., Giardino, A., and Feyen, L. (2016). Projections of extreme storm surge levels along Europe. *Clim. Dyn.* 47, 3171–3190. doi: 10.1007/s00382-016-3019-5

Wang, A. J., Gao, S., and Yang, Y. (2004). Sediment distribution and shape characteristics of gravel beaches, Zhujiajian Island, Zhejiang Province. *J. Nanjing Univ. Nat. Sci.* 40, 747–758. (In Chinese with English abstract).

Wang, H. X., Lu, H. X., and Liang, H. Y. (1998). Analysed storm surge's characteristics along the coast of Hainan Island. *Mar. Forecasts.* 15, 34–42.

Wang, S., Guan, Y., Guan, T., and Huang, J. P. (2012). Oscillation in frequency of tropical cyclones passing Taiwan and Hainan Islands and the relationship with summer monsoon, Chinese. *J oceanol. Limn*. 30, 966–973. doi: 10.1007/s00343-012-1274-9

Wang, Y., Yang, Y., Zhou, L., Wang, Y. P., and Gao, S. (2021). Interpreting the origin of coastal boulders on a coral reef flat at Xiaodonghai, Hainan Island, based on storm wave energy analysis. *J. Trop. Oceanogr.* 40, 110–121. (In Chinese with English abstract). doi: 10.11978/2020093

Woodruff, J. D., Donnelly, J. P., and Okusu, A. (2009). Exploring typhoon variability over the mid-to-late Holocene: evidence of extreme coastal flooding from Kamikoshiki, Japan. *Quat. Sci. Rev*. 28, 1774–1785. doi: 10.1016/j.quascirev.2009.02.005

Wu, Y., Wu, S., and Zhai, P. (2007). The impact of tropical cyclones on Hainan Island's extreme and total precipitation. *Int. J. Climatol*. 27, 1059–1064. doi: 10.1002/joc.1464

Xie, W., He, Q., Zhang, K., Guo, L., Wang, X., Shen, J., et al. (2017). Application of terrestrial laser scanner on tidal flat morphology at a typhoon event timescale. *Geomorphology* 292, 47–58. doi: 10.1016/j.geomorph.2017.04.034

Yang, D. Y., Han, M., Kim, J. C., Cho, Y. K., Kim, J. Y., Yi, S., et al. (2017). Shell and gravel layers caused by storm-induced ripcurrents during the medieval warm period and Little Ice Age in South Korea. *Palaeogeogr. Palaeoclim. Palaeoecol*. 487, 204–215. doi: 10.1016/j.palaeo.2017.08.035

Yao, G. Q., Ding, B. C., Wang, J. Y., and Ma, Z. X. (1991). Statistic analysis on the annual extreme wave parameters of Chinese South Sea. *J. Nanjing Hydraul. Res. Inst.* 141–150.

Ye, L., Wang, X. N., and Bao, C. L. (1994). Tsunami in the China Seas and its warning service. *J. Nat. Disast.* 3, 100–103.

Yin, H. Q. (2014). *Typhoon wave forecast in the South China Sea by SWAN model* (Master thesis). Dalian University of Technology, Dalian, China.

Yu, K. F., Zhao, J., Roff, G., Lybolt, M., Feng, Y., Clark, T., et al. (2012). High-precision U-series ages of transported coral blocks on heron reef (southern great barrier reef) and storm activity during the past century. *Palaeogeogr. Palaeocl*. 337, 23–36. doi: 10.1016/j.palaeo.2012.03.023

Yu, K. F., Zhao, J. X., Collerson, K. D., Qi, S., Chen, T. G., Wang, P. X., et al. (2004). Storm cycles in the last millennium recorded in yongshu reef, southern south china sea. *Palaeogeogr. Palaeoclim. Palaeoecol*. 210, 89–100. doi: 10.1016/j.palaeo.2004.04.002

Yu, K. F., Zhao, J. X., Shi, Q., and Meng, Q. S. (2009). Reconstruction of storm/tsunami records over the last 4000 years using transported coral blocks and lagoon sediments in the southern South China Sea. *Quatern. Int.* 195, 128–137. doi: 10.1016/j.quaint.2008.05.004

Yu, Y., Dong, C., Shan, H., and Zou, B. (2019). Statistical analysis of intensity variations in tropical cyclones in the East China Sea passing over the kuroshio. *J. Oceanol. Limnol*. 38, 1632–1639. doi: 10.1007/s00343-019-9069-x

Yue, Y., Yu, K., Tao, S., Zhang, H., Liu, G., Wang, N., et al. (2019). 3500 year western Pacific storm record warns of additional storm activity in a warming warm pool. *Palaeogeogr. Palaeocl*. 521, 57–71. doi: 10.1016/j.palaeo.2019.02.009

Zhang, Q. (2001). On biogeomorphology of Luhuitou fringing reef of Sanya city, Hainan Island, China. *Chinese Sci. Bull*. 46, 97–101. doi: 10.1007/BF03187245

Zhao, X. T., Zhang, J. W., and Li, G. Y. (1983). Development of the Holocene coral reefs along the southern coast of Hainan Island, *Sci. Geolo. Sin.* 150–158.

Zhou, L., Gao, S., Jia, J., Zhang, Y., Yang, Y., Mao, L., et al. (2019b). Extracting historic cyclone data from coastal dune deposits in eastern Hainan Island, China. *Sediment. Geol*. 392:105524. doi: 10.1016/j.sedgeo.2019.105524

Zhou, L., Yang, Y., Wang, Z., Jia, J., Mao, L., Li, Z., et al. (2019a). Investigating ENSO and WPWP modulated typhoon variability in the South China Sea during the mid–late Holocene using sedimentological evidence from southeastern Hainan Island, China. *Mar. Geol*. 416:105987. doi: 10.1016/j.margeo.2019.105987

Zhou, Q. H., and Adams, W. M. (1988). Tsunami risk analysis for China. *Nat. Hazards* 1, 181–195. doi: 10.1007/BF00126614

Zhou, X., Liu, Z., Yan, Q., Zhang, X., Yi, L., Yang, W., et al. (2019). Enhanced tropical cyclone intensity in the western North Pacific during warm periods over the last two millennia. *Geophys. Res. Lett*. 46, 9145–9153. doi: 10.1029/2019GL083504

Zingg, T. (1935). Beitrag zur Schotteranalyse: Schweizefische Mineralogische und Petrologische. *Mitteilungen* 15, 39–140.

Conflict of Interest: The authors declare that the research was conducted in the absence of any commercial or financial relationships that could be construed as a potential conflict of interest.

Publisher's Note: All claims expressed in this article are solely those of the authors and do not necessarily represent those of their affiliated organizations, or those of the publisher, the editors and the reviewers. Any product that may be evaluated in this article, or claim that may be made by its manufacturer, is not guaranteed or endorsed by the publisher.